IEEE Access
Multidisciplinary | Rapid Review | Open Access Journal

Received March 4, 2021, accepted March 18, 2021, date of publication March 24, 2021, date of current version April 5, 2021.

Digital Object Identifier 10.1109/ACCESS.2021.3068747

Extended State Observer-Based IMC-PID Tracking Control of PMLSM Servo Systems

YACHAO LIU, JIAN GAO, YONGBIN ZHONG, AND LANYU ZHANG
State Key Laboratory of Precision Electronic Manufacturing Technology and Equipment, Guangdong University of Technology, Guangzhou 510006, China
Corresponding author: Lanyu Zhang (lanyuzhang@gdut.edu.cn)

This work was supported in part by the National Natural Science Foundation under Grant 52075106 and Grant U20A6004, and in part by the Guangdong Provincial Research and Development Key Projects under Grant 2018B090906002.

ABSTRACT Servo systems driven by a permanent magnet linear synchronous motor (PMLSM) are often affected by uncertain disturbances, such as magnetic resistance, friction, and external disturbances, which increase tracking errors and reduce motion accuracy. Traditional control methods may have difficulty to achieve satisfactory control performance in terms of tracking accuracy and disturbance rejection. In this paper, we propose an internal model control PID method based on a model linear extended state observer, which is termed as IMC-PID-MLESO method. With this method, the nominal model parameters of the PMLSM servo system are obtained via system identification. The model linear extended state observer (MLESO), with known parameter information, is designed to improve the estimation accuracy for the system states and total unknown uncertainties. As the uncertainties are compensated in the feedback control law, the PMLSM servo system model is transformed into a known nominal model. Based on the nominal model, the IMC-PID feedback controller is designed to ensure satisfactory performance on disturbance rejection and tracking error reduction. Simulation and experimental results show that the IMC-PID-MLESO method can effectively improve the position tracking accuracy of the PMLSM servo system and rapidly suppress the system disturbance.

INDEX TERMS Disturbance suppression, internal model control, permanent magnet linear synchronous motor, tracking accuracy, uncertainties.

I. INTRODUCTION

Permanent magnet linear synchronous motor (PMLSM) servo systems directly drive the mechanism for linear motion in modern industrial automation equipment, such as numerical control machines, industrial robots, laser machining systems, and semiconductor packaging systems. PMLSM servo systems are widely used as they offer a large thrust, fast response, and high precision [1]–[3]. However, uncertain disturbances, such as friction, magnetic resistance, and external disturbances directly affect the mover of a PMLSM without attenuation, leading to substantial tracking errors and complex disturbances during motor movements. This increases the difficulty of controlling the PMLSM servo system and degrades the operational performance [4], [5]. With increasingly stringent requirements in terms of operational efficiency and machining quality, simultaneous reduction in motion tracking errors and disturbances has become a key technical requirement.

Some advanced nonlinear control methods are used to deal with model uncertainties and disturbances, such as model predictive control [6], [7], disturbance observer-robust control [8], sliding mode control [9], [10], adaptive neural network [11], [12], composite anti-disturbance control [13], and so on. However, these methods are more complex and have difficulty to be implemented for motor servo system. At present, the proportional-integral-derivative (PID) controller, which has a simple structure, high practicability, and an independent controlled object model, is the mainstream control strategy for motor servo systems [14]. However, with the development of high-end electronic manufacturing equipment and precision testing equipment, the requirements for motor motion control performance are becoming increasingly stringent, and the traditional PID control structure cannot achieve satisfactory control results [15]. In the past, the combination of PID and advanced control methods and PID parameter optimization are always the research hotspots in the field of

The associate editor coordinating the review of this manuscript and approving it for publication was Jingang Jiang.

control engineering. On the one hand, some nonlinear PID control strategies, such as fractional PID [16], [17], neural network PID [18], [19], neural fuzzy PID [20], [21], and particle swarm optimization PID [22], [23] have been proposed. On the other hand, it is particularly important to adjust the PID controller parameters appropriately, using methods such as the well-known Ziegler–Nichols (ZN) tuning rule [24], H_2/H_∞ robust optimization design [25], internal model control (IMC) principle [26], and other parameter adjustment methods [27], [28]. Among these, PID controllers based on the IMC principle are recognized as the simplest and most effective controllers for tuning [29], [30]. In particular, when the model of the controlled object is ideal and external disturbances are absent, the internal model control PID (IMC-PID) controller can achieve satisfactory target instruction tracking performance. However, the PMLSM itself has strong nonlinearity and coupling, which causes accurate modeling of the system to be difficult. Hence, modeling errors and un-modeled dynamics are inevitable, and changes in load resistance result in additional external disturbances [31], [32]. As IMC-PID is a single degree-of-freedom control strategy, it is difficult to improve the tracking and disturbance rejection performance of a PMLSM servo system. Therefore, it is necessary to design an effective control strategy to improve the disturbance rejection ability of PMLSM servo systems, and without sacrificing the precision tracking performance of the IMC-PID controller.

Among the disturbance rejection methods, active disturbance rejection control (ADRC), a new type of strong anti-interference control technology based on nonlinear PID, has been widely studied for position tracking and disturbance rejection of motor servo systems [33], [34]. ADRC does not require a precise mathematical model of the controlled object, as its core idea is to build an extended state observer (ESO) to estimate the total uncertain disturbances both inside and outside the system in real-time, and to compensate for the disturbance dynamically. Thus, the controlled object model is transformed into integral series standard form. However, the conventional ADRC method involves nonlinear links, which complicates the settings and necessitates several parameter adjustments [35]. The linear active disturbance rejection control (LADRC) structure uses the mathematical form of a linear ESO (LESO), making ADRC widely usable in engineering applications [36]. For systems with parameter uncertainties and disturbances, some ESO-based control methods have been studied. For example, a practical ADRC algorithm for hydraulic servo system without resorting to the identification model was developed in [37], which achieved good control responses. A compound control strategy that combines ADRC and velocity compensation for electro-hydraulic position servo control system was proposed in [38], which improved the anti-interference ability and control precision of the system. The ESO-based control method had been well implemented in these complex systems, which provided valuable experience for application in motor control occasions.

In recent years, many scholars have designed effective control methods for motor servo systems based on LADRC [39]–[41]. In [39], LADRC was used for disturbance control of a permanent magnet synchronous generator to improve the tracking accuracy of the servo system. In [40], an LADRC method for measuring delay compensation of permanent magnet synchronous motor (PMSM) current loop was proposed; this method improves the disturbance suppression performance under the dead-time effect. In [41], a control strategy based on fractional order ESO was proposed for a PMSM position servo system; this strategy improves the motion accuracy and disturbance rejection ability. It can be seen from the existing research work that adding known model information into ESO design can reduce observation burden and improve estimation accuracy of system states [42], [43]. In [44], an ADRC scheme based on model compensation for PMSM speed regulation system was proposed, which improved the estimation accuracy of the total disturbances. In [45], the identified disturbance model was compensated to ADRC, which had stronger anti-interference ability of PMSM speed control system.

In [46], a compound control method combining IMC and ESO was proposed to improve the set-point tracking performance and disturbance rejection ability of a PMSM servo system. However, the identified model parameters were not fully utilized in designing the ESO in [46], and parameter setting of ESO was directly transplanted the traditional bandwidth setting rules, which was not rigorous. In addition, the PMLSM servo system is more sensitive to disturbances than PMSM servo system, so the ESO design method should be further developed with stronger disturbance estimation ability. Hence, to achieve simultaneous tracking error compensation and disturbance suppression in PMSLM servo systems, in this study, the advantages of IMC and LADRC are combined, and an internal model control PID based on the model linear extended state observer (IMC-PID-MLESO) is proposed. This method involves system identification to obtain the nominal model parameters of a PMLSM servo system and uses a model linear expansion state observer (MLESO) that integrates known parameter information to improve the estimation accuracy for the unknown total uncertainties. On the basis of compensating for the unknown total uncertainties, the PMLSM servo system model is transformed into a known nominal model, and the IMC-PID feedback controller of this model is designed accordingly. The contributions of this work can be summarized as follows:

(1) The design of MLESO and its parameter tuning can make full use of the known model information. The complex PMLSM servo system model can be transformed into a known nominal model, which is perfectly combined with the IMC-PID controller design method.

(2) The proposed control method can ensure the BIBO stability of the system and have good tracking performance. Simulation and experiment show that the method can suppress the disturbances of PMLSM servo system quickly and has smaller tracking error.

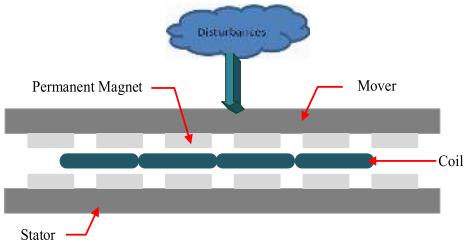

FIGURE 1. Structure of PMLSM without an iron core.

The remainder of this paper is organized as follows. In Section II, the modeling process of the PMLSM servo system is introduced. In Section III, the control strategy for the PMLSM servo system is described, including the MLESO design, nominal model transformation process, IMC-PID controller design, and stability proof of the closed-loop system. Section IV compares the results of simulation analyses for the relevant methods, with respect to the identified nominal model. Section V describes the dSPACE experimental system of the PMLSM platform and presents the verification of the effectiveness of the proposed method. Finally, the conclusions are presented in Section VI.

II. MATHEMATICAL MODEL OF PMLSM SERVO SYSTEM

The PMLSM is vulnerable to various disturbances during its operation, which negatively affect the mover. The structure of a PMLSM without an iron core is shown in Fig. 1.

Ignoring the influence of eddy currents and hysteresis loss and assuming that the three-phase current is sinusoidal, the mathematical model of the PMLSM is established in the $d-q$ coordinate system and is expressed as

$$\begin{cases} u_d = Ri_d + L_d\dot{i}_d - \dfrac{\pi v}{\tau}L_q i_q \\ u_q = Ri_q + L_q\dot{i}_q + \dfrac{\pi v}{\tau}\left(L_d i_d + \psi_{PM}\right) \\ F_e = \dfrac{3\pi}{2\tau}\left[\psi_{PM} i_q + \left(L_d - L_q\right) i_d i_q\right] \end{cases} \tag{1}$$

where R is the winding resistance of the mover. i_d, i_q, u_d, u_q, L_d, and L_q are the current, voltage, and inductance of the d and q axes, respectively, ψ_{PM} is the flux linkage of the permanent magnet, v is the speed of the mover, and τ is the motor pole distance, and F_e is the electromagnetic thrust.

Because the air gap of the linear motor is large, it is generally considered that the inductances in the d and q axes are the same, that is, $L_d = L_q = L$. In the vector control mode, the reference input current in the d axis is $i_d = 0$. Hence, the expression of electromagnetic thrust can be simplified as

$$F_e = K_f i_q \tag{2}$$

where K_f is the thrust coefficient, $K_f = 3\pi n_p \psi_{PM}/(2\tau)$. If external uncertainties such as load disturbance and environmental noise are not considered, the mechanical motion equation of the PMLSM can be expressed as

$$F_e = M\dot{v} + Bv + F_d \tag{3}$$

where M is the moving mass of the mover, B is the coefficient of viscous friction, and F_d is the internal multiple disturbing force of the motor, including sliding friction and magnetic resistance. In the analog current loop, we have $i_q = K_q u$, where i_q is the reference input current in the q axis, and K_q is the scaling factor. According to its response characteristics, we approximate the current loop as a unit proportional link, combining (2)–(3), and let $a_0 = B/M$, and $b_0 = K_f K_q/M$. Finally, the dynamic equation of the PMLSM servo system with the current loop is obtained as follows

$$\begin{aligned} \ddot{x} &= -\left(a_0 + \Delta a\right)\dot{x} + \left(b_0 + \Delta b\right)u \\ &= -a\dot{x} + bu \end{aligned} \tag{4}$$

where $a = a_0 + \Delta a$, $b = b_0 + \Delta b$, x is the movement displacement of the PMLSM, u is the control input voltage, and Δa and Δb are the parameter uncertainties of $\dot{x}$ and u introduced by multiple disturbing forces F_d, respectively. Here, $-\Delta a\dot{x} + \Delta b u \triangleq -F_d/M$ is defined.

III. CONTROL STRATEGY OF PMLSM SERVO SYSTEM

A. MLESO DESIGN AND NOMINAL MODEL MODIFICATION

As the concept of total uncertainties f in LADRC include both known and unknown disturbances. For PMLSM servo system (4), $f = -a\dot{x} + \left(b - \hat{b}\right)u + w$, where $\hat{b}$ is the estimated value of b, w is external unknown uncertainties. The time derivative of function f is bounded because the speed of disturbance change cannot be infinitely fast in any real physical system. We define that the total unknown uncertainties is $h = -\left(a - a_n\right)\dot{x} + \left(b - b_n\right)u + w = f + a_n\dot{x} + \left(\hat{b} - b_n\right)u$, where a_n and b_n are the nominal values of parameters a and b, respectively, which are obtained via system identification. It can be seen that the time derivative of function h is bounded. Let the system state variables be $x_1 = x$, $x_2 = \dot{x}$, and $x_3 = h$. Then, the state space equation of the PMLSM servo system (4) in the extended state is

$$\begin{cases} \dot{\boldsymbol{X}} = \boldsymbol{A}\boldsymbol{X} + \boldsymbol{B}u + \boldsymbol{E}\dot{h} \\ x = \boldsymbol{C}\boldsymbol{X} \end{cases} \tag{5}$$

where $\boldsymbol{X} = \begin{bmatrix} x_1 \\ x_2 \\ x_3 \end{bmatrix}$, $\boldsymbol{A} = \begin{bmatrix} 0 & 1 & 0 \\ 0 & -a_n & 1 \\ 0 & 0 & 0 \end{bmatrix}$, $\boldsymbol{B} = \begin{bmatrix} 0 \\ b_n \\ 0 \end{bmatrix}$, $\boldsymbol{E} = \begin{bmatrix} 0 \\ 0 \\ 1 \end{bmatrix}$, $\boldsymbol{C} = \begin{bmatrix} 1 & 0 & 0 \end{bmatrix}$. According to system (5), the third-order MLESO can be designed as

$$\begin{cases} \dot{\hat{\boldsymbol{X}}} = \boldsymbol{A}\hat{\boldsymbol{X}} + \boldsymbol{B}u + \boldsymbol{L}\left(x - \hat{x}_1\right) \\ \hat{x}_1 = \boldsymbol{C}\hat{\boldsymbol{X}} \end{cases} \tag{6}$$

where $\hat{\boldsymbol{X}} = \begin{bmatrix} \hat{x}_1 & \hat{x}_2 & \hat{x}_3 \end{bmatrix}^T$ is the state estimation vector of $\boldsymbol{X}$, $\boldsymbol{L} = \begin{bmatrix} l_1 & l_2 & l_3 \end{bmatrix}^T$ is the observer gain vector. The state estimation error is

$$\dot{\boldsymbol{X}} - \dot{\hat{\boldsymbol{X}}} = \left(\boldsymbol{A} - \boldsymbol{L}\boldsymbol{C}\right)\left(\boldsymbol{X} - \hat{\boldsymbol{X}}\right) + \boldsymbol{E}\dot{h} \tag{7}$$

To ensure that the estimation error can converge to zero, the matrix $(\boldsymbol{A} - \boldsymbol{LC})$ must be Hurwitz. In order to satisfy this condition, let the characteristic polynomial of the matrix be

$$|s\boldsymbol{I} - (\boldsymbol{A} - \boldsymbol{LC})| = (s + w_o)^3 \tag{8}$$

From (8), the following tuning rules are obtained

$$l_1 = 3w_o - a_n;\ l_2 = 3w_o^2 - 3w_o a_n + a_n^2;\ l_3 = w_o^3 \tag{9}$$

By (9) and (12), we have

$$\begin{cases} \dot{\tilde{x}}_1 = \tilde{x}_2 - (3w_o - a_n)\,\tilde{x}_1 \\ \dot{\tilde{x}}_2 = \tilde{x}_3 - a_n\tilde{x}_2 - \left(3w_o^2 - 3w_o a_n + a_n^2\right)\tilde{x}_1 \\ \dot{\tilde{x}}_3 = \dot{h} - w_o^3\tilde{x}_1 \end{cases} \tag{10}$$

where $\tilde{x}_i = x_i - \hat{x}_i,\ i = 1, 2, 3$. To prove the convergence of the MLESO, the following two assumptions are used.

Assumption 1: There exists $T_1 > 0$, when $t > T_1$ such that $\left|\dot{h}\right| \le \delta,\ \delta > 0$.

Assumption 2: There exists $T_2 > 0$, when $t > T_2$ such that system (10) enters a steady state, that is, $\dot{\tilde{x}}_1 = \dot{\tilde{x}}_2 = \dot{\tilde{x}}_3 = 0$.

Combining Assumption 1 and Assumption 2, the following formula is obtained:

$$|\tilde{x}_1| \le \frac{\delta}{w_o^3};\ |\tilde{x}_2| \le \frac{|3 - a_n/w_o|\,\delta}{w_o^2};\ |\tilde{x}_3| \le \frac{3\delta}{w_o} \tag{11}$$

Let $\sigma_1 = \delta/w_o^3$, $\sigma_2 = |3 - a_n/w_o|\,\delta/w_o^2$, $\sigma_3 = 3\delta/w_o$. Then, we obtain the following theorem.

Theorem 1: Consider the system described by (6), which satisfies Assumption 1 and Assumption 2. Then, there is a large enough positive number w_o such that state estimation error $|\tilde{x}_i(t)| \le \sigma_i,\ i = 1, 2, 3$, where $\sigma_i = o\left(1/w_o^c\right),\ i = 1, 2, 3$, c is a positive integer.

Remark 1: According to Theorem 1, the state estimation error of MLESO is related to w_o. When w_o is larger, the state estimation error $\tilde{x}_i$ is smaller, and the observation response is faster. However, in an actual system, w_o is limited by the measurement noise and other factors. If w_o is excessively large, high-frequency noise disturbances will be introduced into the system, and degrading the quality of the state estimation variables.

The estimated total unknown uncertainties $\hat{x}_3$ are dynamically compensated in the control law, as follows

$$u = u_0 - \frac{\hat{x}_3}{b_n} \tag{12}$$

where u_0 is the initial control value calculated using the error feedback controller. We choose an appropriate observer bandwidth w_o to ensure that $\hat{x}_3$ can be accurately estimated h, then

$$\begin{aligned} \ddot{x} &= -a_n x_2 + x_3 + b_n u_0 - \hat{x}_3 \\ &\approx -a_n\dot{x} + b_n u_0 \end{aligned} \tag{13}$$

Therefore, through real-time estimation of the MLESO and based on the dynamically compensated control law, the PMLSM servo system model (4) is approximately transformed into the nominal model (13).

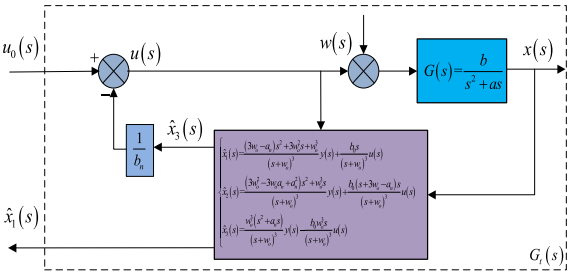

FIGURE 2. Transformation process of controlled object model.

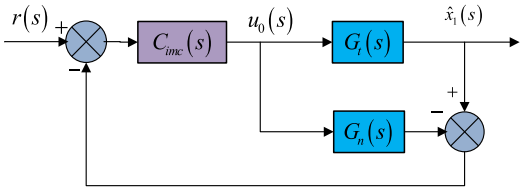

FIGURE 3. Block diagram of IMC control structure.

Remark 2: Compared with the traditional LADRC, the proposed method has the following advantages: 1) The nominal model information obtained via the identification is fully utilized, which can improve the control performance of LADRC; 2) The upper limit of the bandwidth of the observer in the actual system is restricted, and it is more feasible to transform the controlled object model into a nominal model than to transform it into a standard integral series form.

B. DESIGN OF IMC-PID CONTROLLER BASED ON MLESO

Hence, the transfer function model between the voltage and displacement of the PMLSM servo system and its nominal model are

$$G(s) = \frac{b}{s^2 + as};\ G_n(s) = \frac{b_n}{s^2 + a_n s} \tag{14}$$

From (6) and (9), the frequency domain representation of MLESO is as follows (15), as shown at the bottom of the next page.

The transformation process is shown in Fig. 2.

In Fig. 2, $G_t(s)$ is the transfer function model between the voltage and the estimated displacement of MLESO. The IMC principle is used to design the IMC-PID feedback controller, and its control structure is shown in Fig. 3.

In Fig. 3, the IMC controller $C_{imc}(s)$ can be designed as follows

$$C_{imc}(s) = \frac{f(s)}{G_n(s)} \tag{16}$$

where $f(s)$ is the internal model filter, which is expressed as

$$f(s) = \frac{2\lambda s + 1}{(\lambda s + 1)^2} \tag{17}$$

where λ is the filter parameter. The filter satisfies the following conditions [23]

$$\lim_{s\to 0}\{[1 - f(s)]\ G_n(s)\} = 0 \tag{18}$$

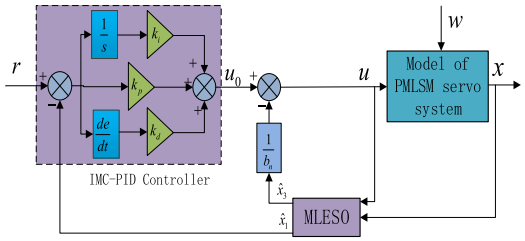

FIGURE 4. IMC-PID control structure based on MLESO.

The closed-loop system transfer function is given as follows

$$\hat{x}_1(s) = \frac{C_{imc}(s) G_t(s)}{1 + C_{imc}(s)[G_t(s) - G_n(s)]} r(s) \tag{19}$$

In the ideal case, there is $G_t(s) = G_n(s)$. Thus, the expected output of the system is

$$x_{1d}(s) = f(s) r(s) \tag{20}$$

Therefore, the closed-loop performance of the IMC-PID controller will be similar to the IMC filter. The desired closed-loop response can be obtained by selecting appropriate IMC filter parameters. The IMC-PID controller is expressed as

$$\begin{aligned} G_{pid}(s) &= \frac{f(s)}{[1 - f(s)] G_n(s)} \\ &= k_p + k_i \frac{1}{s} + k_d s \end{aligned} \tag{21}$$

where k_c, k_i and k_d are the proportional, integral and differential coefficients, respectively. From (24), the parameter setting rules of the IMC-PID controller are obtained as follows

$$k_p = \frac{2\lambda a_n + 1}{\lambda^2 b_n}; k_i = \frac{a_n}{\lambda^2 b_n}; k_d = \frac{2}{\lambda b_n} \tag{22}$$

The nominal parameters a_n and b_n of the system are obtained by model identification, so the proposed method only needs to adjust two control parameters, i.e., the observer bandwidth w_o of MLESO and filter parameter λ of IMC-PID. The structure of the proposed IMC-PID-MLESO of the PMLSM servo system is shown in Fig. 4. In the expected case, the IMC-PID-MLESO equivalent control structure is obtained, as shown in Fig. 5.

Finally, the initial control value calculated by the IMC-PID controller is

$$u_0(s) = G_{pid}(s)\left[r(s) - \hat{x}_1(s)\right] \tag{23}$$

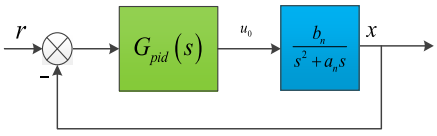

FIGURE 5. Equivalent control structure of IMC-PID-MLESO.

Remark 3: Based on (11), the estimation error of the state velocity will be considerably larger than the displacement estimation error when w_o is sufficiently large. Thus, the use of velocity estimation signal is debatable. Unlike the LADRC method, the IMC-PID-MLESO method designed in this study only takes the displacement estimation variable as the feedback signal of the controller in (23), to avoid the lag effect of the speed estimation signal.

C. STABILITY ANALYSIS

This part analyzes the bounded-input bounded-output (BIBO) stability of IMC-PID-MLESO closed-loop control system. The following theorem is given.

Theorem 2: When the state estimation error of the MLESO is bounded, that is, $|\tilde{x}_i(t)| \leq \sigma_i, \sigma_i > 0, i = 1, 2, 3$, there exists a filter parameter $\lambda > 0$ for any bounded input r, such that the closed-loop system composed of IMC-PID-MLESO is bounded-input bounded-output stable.

Proof: From (20), the expected output of the system is

$$x_{1d} = 2\lambda \dot{r} + r - \lambda^2 \ddot{x}_{1d} - 2\lambda \dot{x}_{1d} \tag{24}$$

The expected error between the actual and expected output of system (6) is defined as $\varepsilon_1 = x_1 - x_{1d}$. From (22), we have

$$\lambda^2 \ddot{x}_{1d} = 2\lambda \Delta \dot{r} + \Delta r \tag{25}$$

where $\Delta r = r - x_{1d}$. Hence,

$$e_1 = \varepsilon_1 - \tilde{x}_1 - \Delta r \tag{26}$$

The intermediate error variable is designed as $\upsilon = a_n \varepsilon_1 + \dot{\varepsilon}_1 = x_2 - x_{2d}$. Let

$$\begin{aligned} \varepsilon_2 &= \upsilon + \frac{1}{\lambda} \int \upsilon dt \\ &= \dot{\varepsilon}_1 + \frac{\lambda a_n + 1}{\lambda} \varepsilon_1 + \frac{a_n}{\lambda} \int \varepsilon_1 dt \end{aligned} \tag{27}$$

Then, the transfer function model between ε_2 and ε_1 is

$$G_\varepsilon(s) = \frac{\lambda s}{(s + a_n)(\lambda s + 1)} \tag{28}$$

$$\begin{cases} \hat{x}_1(s) = \dfrac{(3w_o - a_n) s^2 + 3w_o^2 s + w_o^3}{(s + w_o)^3} y(s) + \dfrac{b_0 s}{(s + w_o)^3} u(s) \\ \hat{x}_2(s) = \dfrac{\left(3w_o^2 - 3w_o a_n + a_n^2\right) s^2 + w_o^3 s}{(s + w_o)^3} y(s) + \dfrac{b_0 (s + 3w_o - a_n) s}{(s + w_o)^3} u(s) \\ \hat{x}_3(s) = \dfrac{w_o^3 \left(s^2 + a_n s\right)}{(s + w_o)^3} y(s) - \dfrac{b_0 w_o^3 s}{(s + w_o)^3} u(s) \end{cases} \tag{15}$$

Because $G_\varepsilon(s)$ is stable, when ε_2 is bounded-output stable, ε_1 is also bounded-output stable. The derivative of ε_2 is

$$\begin{aligned}\dot{\varepsilon}_2 &= \dot{\upsilon} + \frac{\upsilon}{\lambda} \\ &= \dot{\tilde{x}}_2 - \dot{x}_{2d} + \frac{a_n\varepsilon_1 + \dot{\varepsilon}_1}{\lambda} \\ &= \gamma_1 + \gamma_2 + \gamma_3 \end{aligned} \tag{29}$$

where

$$\gamma_1 = -b_n\left(k_p\varepsilon_1 + k_i\int\varepsilon_1 dt + k_d\dot{\varepsilon}_1\right) + \frac{a_n\varepsilon_1 + \dot{\varepsilon}_1}{\lambda}$$

$$\gamma_2 = b_n\left(k_p\Delta r + k_i\int\Delta r dt + k_d\Delta\dot{r}\right) - a_n x_2 - \dot{x}_{2d}$$

$$\gamma_3 = b_n\left(k_p\tilde{x}_1 + k_i\int\tilde{x}_1 dt + k_d\dot{\tilde{x}}_{11}\right) + \tilde{x}_3$$

By simplifying (32) further, we obtain

$$\gamma_1 = -\frac{1}{\lambda}\varepsilon_2 \tag{30}$$

$$\gamma_2 = 0 \tag{31}$$

From Theorem 1, we have

$$\gamma_3 \le b_n\left(k_p\sigma_1 + k_i\int\sigma_1 dt\right) + \sigma_3 = \sigma \tag{32}$$

Then,

$$\dot{\varepsilon}_2 \le -\frac{1}{\lambda}\varepsilon_2 + \sigma \tag{33}$$

Solving (33), we have

$$\begin{aligned}\varepsilon_2(t) &\le e^{-\int_{T_1}^{t}\frac{1}{\lambda}dx}\left[\int_{T}^{t}\sigma e^{\int_{T_1}^{\tau}\frac{1}{\lambda}d\tau}dx + \varepsilon_2(T_1)\right] \\ &\le \varepsilon_2(T_1)e^{-\frac{t-T_1}{\lambda}} + \lambda\sigma\left(1 - e^{-\frac{t-T_1}{\lambda}}\right)\end{aligned} \tag{34}$$

Then,

$$|\varepsilon_2(t)| < |\varepsilon_2(T_1)| + \lambda\sigma = \sigma_4 \tag{35}$$

Therefore, for an arbitrary bounded input r, the closed-loop system composed of IMC-PID-MLESO is BIBO stable. This completes the proof of Theorem 2. In addition, decreasing λ or increasing w_o can reduce the tracking error.

Remark 4: It can be seen from (13) that the transformed model is an observable and controllable linear time invariant system, so the BIBO stability is consistent with the asymptotic stability. Therefore, when the system is BIBO stable, the controller can obtain good tracking performance.

IV. SIMULATION RESULTS

The system identification for the PMLSM servo system model is conducted through a sinusoidal frequency sweep experiment, and the nominal values of system (8) are $a_n = 7.655$, $b_n = 2.57$. To verify the control performance of the IMC-PID-MLESO, its control results are compared with those of the IMC-PID (without MLESO) and LADRC. For a fair comparison, the MLESO and LESO have the same observer bandwidth, that is, $w_o = 150$, while the controller bandwidth of LADRC is $w_c = 200$. IMC-PID-MLESO and IMC-PID have the same filter parameter, that is, $\lambda = 0.005$. The aforementioned methods are simulated and analyzed in the MATLAB environment.

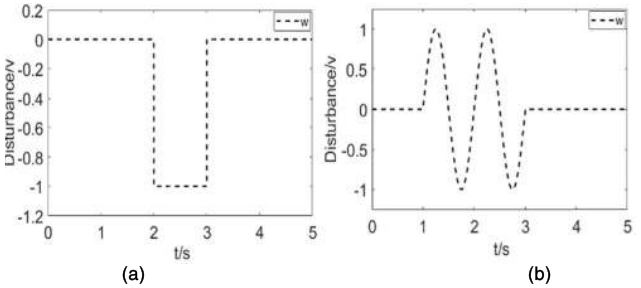

FIGURE 6. Forms of external disturbance used to verify the control performance of the proposed method: (a) step disturbance, (b) sinusoidal disturbance.

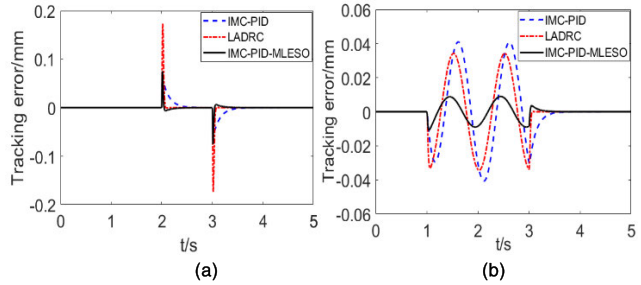

FIGURE 7. Tracking errors of external disturbance: (a) step disturbance, (b) sinusoidal disturbance.

A. SIMULATION OF EXTERNAL DISTURBANCE SUPPRESSION

After the steady state of reaching the target value, external disturbances are applied, as shown in Fig. 6(a) and 6(b). The action time of the step disturbance voltage is 2–3s and the amplitude is −1V. The action time of the sinusoidal disturbance voltage is 1–3s, and the amplitude is −1V. The corresponding disturbance tracking errors obtained via simulation are shown in Fig. 7(a) and 7(b).

It can be seen that the proposed IMC-PID-MLESO method could rapidly suppress the disturbance and that its disturbance rejection performance is clearly superior to that of IMC-PID and LADRC.

B. TRACKING RESPONSE OF REFERENCE INPUT

First, the nominal model is assumed to be ideal, that is, $G_n(s) = G(s)$. The trajectory planning signal has the following parameters: Stroke $s_t = 10$mm, maximum velocity $v_{\max} = 0.1$m/s, and maximum acceleration $a_{\max} = 10$m/s^2. These values are taken as the reference input for set-point tracking. A constant external input voltage disturbance with the amplitude of −1V is added at $t = 2.5$s. The tracking error of the system is shown in Fig. 8.

Fig. 8 shows that in the ideal model, the dynamic tracking performance of IMC-PID and IMC-PID-MLESO is almost

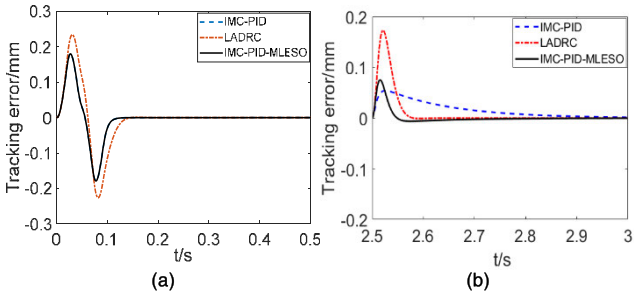

FIGURE 8. Set-point tracking error under ideal model: (a) dynamic response error, (b) disturbance rejection error.

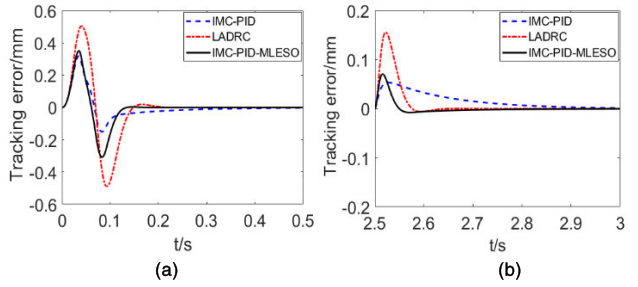

FIGURE 9. Set-point tracking errors under $a = 5a_n$: (a) dynamic response error, (b) disturbance rejection error.

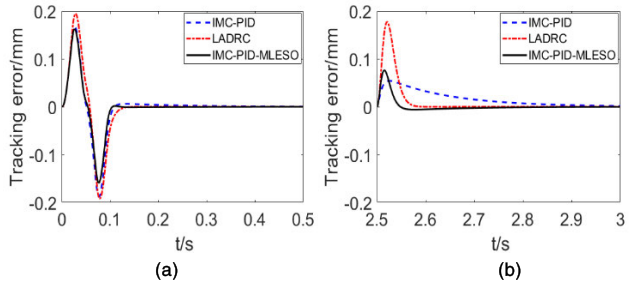

FIGURE 10. Set-point tracking errors under $a = 0.2a_n$: (a) dynamic response error, (b) disturbance rejection error.

identical, but the ability of IMC-PID to suppress the constant disturbance is poor. Although the tracking error of LADRC is large, it can suppress the disturbance quickly. Because the estimation accuracy of the MLESO is higher than that of the LESO for the same observer bandwidth, the disturbance error of IMC-PID-MLESO is smaller, and its suppression time is shorter than that of LADRC.

The control parameters, reference input, and external disturbance are kept unchanged, and the tracking responses are compared when the internal parameters of the system are uncertain. First, we separately consider two types of parameter uncertainties when $a = 5a_n$ and $a = 0.2a_n$. The tracking error and disturbance rejection obtained via the simulation are shown in Figs. 9 and 10. Then, we consider two types of parameter uncertainties when a and b change simultaneously, that is, $a = 5a_n$, $b = 2b_n$ and $a = 0.2a_n$, $b = 0.5b_n$. The tracking error is shown in Figs. 11 and 12.

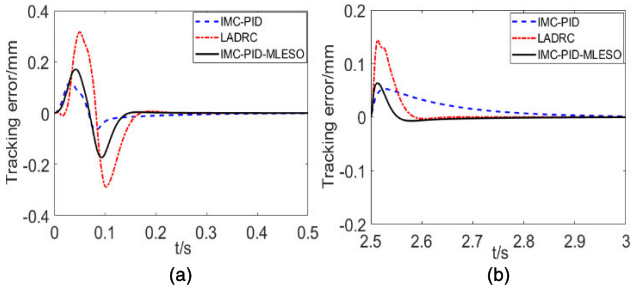

FIGURE 11. Set-point tracking errors under $a = 5a_n$ and $b = 2b_n$: (a) dynamic response error, (b) disturbance rejection error.

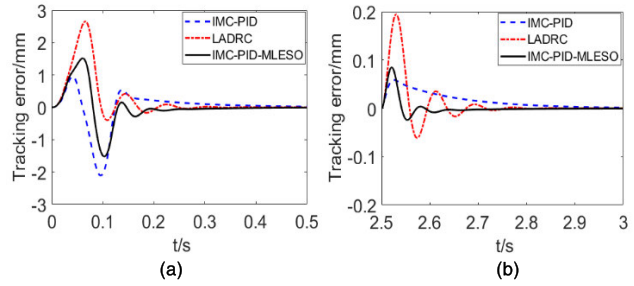

FIGURE 12. Set-point tracking errors under $a = 0.2a_n$ and $b = 0.5b_n$: (a) dynamic response error, (b) disturbance rejection error.

It can be seen from Figs. 9–12 that IMC-PID-MLESO achieves the best tracking performance for the four parameter uncertainties with the given reference input. Moreover, it can quickly reach the target value, which indicates that it can suppress internal parameter disturbances effectively. The adjustment process for IMC-PID is relatively slow, while LADRC has a large tracking error. In addition, for external voltage disturbances, IMC-PID-MLESO exhibits a smaller disturbance error and shorter disturbance rejection time than IMC-PID and LADRC.

C. TRACKING RESPONSE OF SINUSOIDAL SIGNAL

With a sinusoidal signal having the amplitude of 5mm and frequencies of 2.5Hz and 5Hz as the reference input, the tracking error curves for the ideal model are obtained via simulation, as shown in Fig. 13. Keeping the reference input and control parameters unchanged, parameter uncertainties of $a = 0.8a_n$ and $b = 0.8b_n$ are introduced, and the tracking error curves are shown in Fig. 14.

Fig. 13 shows that in the ideal model, the tracking performance of LADRC is poor, while the tracking errors of IMC-PID and IMC-PID-MLESO are highly consistent. Fig. 14 shows that when the parameter uncertainty is introduced, the tracking performance of IMC-PID deteriorates slightly, while IMC-PID-MLESO continues to perform satisfactory control.

In summary, the simulation results show that a PID controller based on the IMC principle can achieve satisfactory tracking control performance but cannot suppress disturbances effectively. In comparison, LADRC has significantly

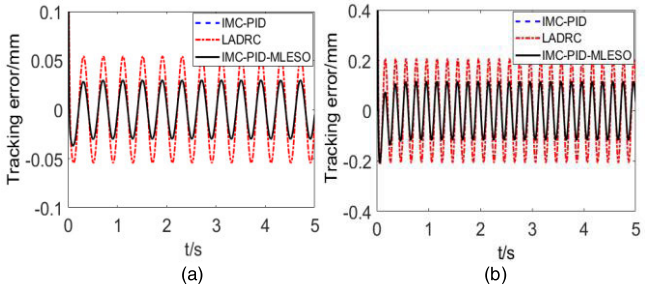

FIGURE 13. Tracking errors of sinusoidal under ideal model: (a) 2.5Hz, (b) 5Hz.

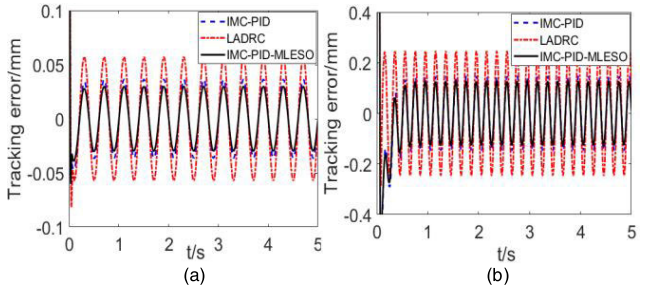

FIGURE 14. Tracking errors of sinusoidal under parameter perturbation: (a) 2.5Hz, (b) 5Hz.

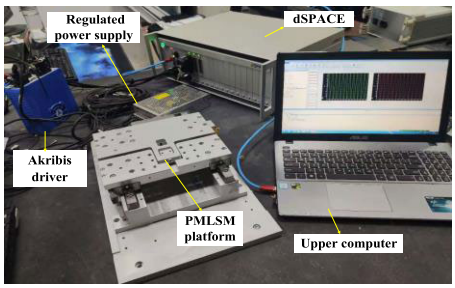

FIGURE 15. Experimental platform with PMLSM servo system.

better disturbance rejection ability, but its tracking performance is unsatisfactory. The proposed IMC-PID-MLESO method can achieve satisfactory tracking performance and disturbance rejection simultaneously, which is suitable for the motion control of PMLSM servo systems.

V. EXPERIMENTAL VERIFICATION

To verify the control performance of the IMC-PID-MLESO for PMLSM servo systems, an experimental platform with a PMSLM servo system based on dSPACE is built in this study, as shown in Fig. 15. In the experiment, a dSPACE DS2655-7K160 controller and a PMLSM with an AUM5-S1 series brushless iron core and an Akribis ASD 240-0418 driver are used. The absolute grating ruler of the experimental platform is an HEIDENHAIN AK LIC411, the feedback resolution is 1μm, and the sampling frequency is 1kHz. To verify the effectiveness of the proposed method, the disturbance rejection and tracking performance of IMC-PID-MLESO is

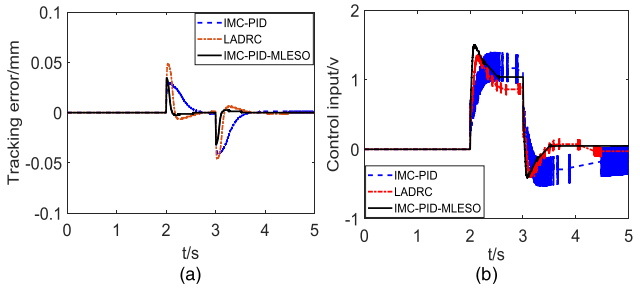

FIGURE 16. Responses under step disturbance: (a) disturbance rejection error, (b) control input.

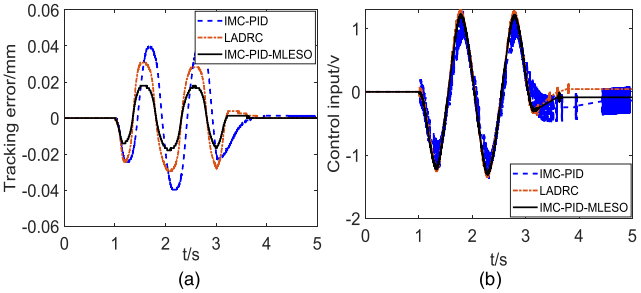

FIGURE 17. Responses under sinusoidal disturbance: (a) disturbance rejection error, (b) control input.

compared with that of IMC-PID and LADRC under the same conditions.

A. DISTURBANCE SUPPRESSION

Under steady-state conditions, the disturbance voltage signals shown in Fig. 6(a) and 6(b) are applied as the external disturbance. The experimental results for the tracking error and control input are shown in Figs. 16 and 17. The maximum tracking error (Max|e|), integral absolute value of the tracking error (IAE), and total variation (TV) in the control input are used as control performance evaluation indexes. The results are shown in Table 1.

It can be seen from Figs. 16 and 17 and from Table 1 that for IMC-PID-MLESO, the Max|e|, IAE, and TV are the smallest under the external step disturbance and that the IAE is 75.7% and 62.9% lower than those of IMC-PID and LADRC, respectively. The Max|e|, IAE, and TV of IMC-PID-MLESO are also the smallest under the external sinusoidal disturbance, and the IAE is 54.0% and 42.1% lower than those of IMC-PID and LADRC, respectively. This shows that IMC-PID-MLESO has the strongest disturbance rejection ability.

B. TRACKING DIFFERENT MOTION STROKES

The friction force of the PMLSM changes depending on the situation of the guide rail, which, in turn, leads to changes in the internal parameters. In this study, keeping the control parameters unchanged, set-point tracking is performed with different stroke lengths, corresponding to the simulation analysis of the uncertain internal parameters of the PMLSM servo system. The maximum stroke used for the experimental

TABLE 1. The control performance indexes under different disturbances.

Method	Step disturbance			Sine disturbance		
	Max|e| (mm)	IAE(10^{-2})	TV	Max|e| (mm)	IAE(10^{-2})	TV
IMC-PID	0.041	2.30	219.7	0.040	5.68	319.7
LADRC	0.049	1.51	37.43	0.031	4.51	56.8
IMC-PID-MLESO	0.035	0.56	7.379	0.018	2.61	45.58

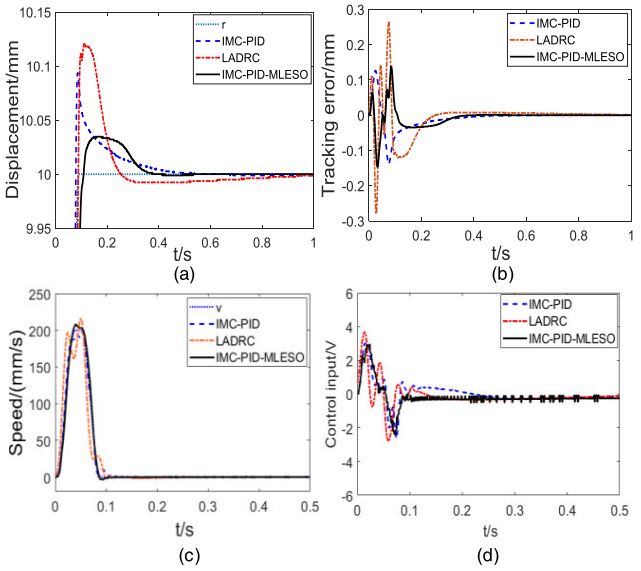

FIGURE 18. Set-point tracking for stroke of 10 mm: (a) output displacement, (b) tracking error, (c) speed, (d) control input.

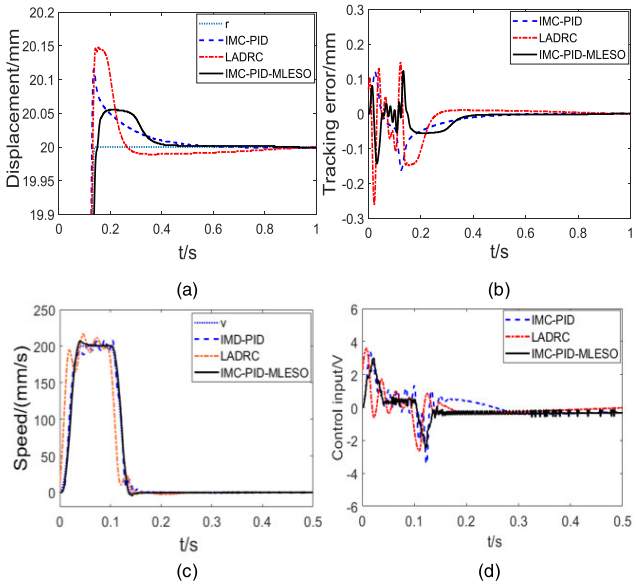

FIGURE 19. Set-point tracking for stroke of 20 mm: (a) output displacement, (b) tracking error, (c) speed, (d) control input.

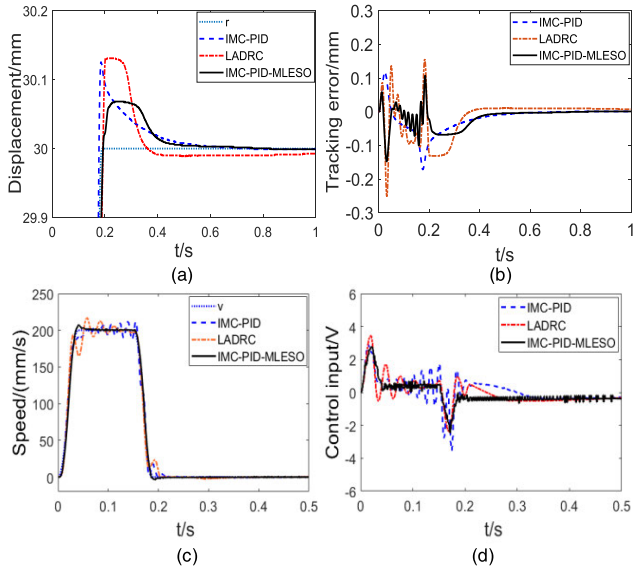

FIGURE 20. Set-point tracking for stroke of 30 mm: (a) output displacement, (b) tracking error, (c) speed, (d) control input.

platform is 40mm, and the motion strokes of the PMLSM are set as s_t = 10mm, 20mm, and 30mm, with a maximum speed $v_{\max}$ = 0.2m/s and maximum acceleration $a_{\max}$ = 10 m/s^2. The experimental results are shown in Figs. 18–20. The setting time (ST), overshoot (OS) and IAE are used as the control performance evaluation indexes, and the results are shown in Table 2.

According to Figs. 18–20 and Table 2, the ST of IMC-PID-MLESO is the smallest. Compared with IMC-PID and LADRC, the ST of IMC-PID-MLESO is reduced by 19.5% and 61.3% for the 10mm stroke, 26.2% and 58.3% for the 20mm stroke, and 14.2% and 68.4% for the 30mm stroke, respectively. The OS and IAE of IMC-PID-MLESO are also the smallest, while those of LADRC are the largest. The speed tracking performance of IMC-PID-MLESO is better than IMC-PID and LADRC. With the increase of stroke, the speed tracking performance of IMC-PID deteriorates obviously. The control input curve of the proposed method is relatively stable without oscillation. This proves that the proposed controller achieves satisfactory set-point tracking performance.

C. TRACKING SINUSOIDAL SIGNALS

Sinusoidal signals with four different amplitudes and frequencies are used as input in the experiment. The following four cases are considered—Case 1: 5mm amplitude and 2.5Hz frequency; Case 2: 5mm amplitude and 5Hz frequency; Case 3: 10mm amplitude and 2.5Hz frequency; Case 4: 10mm amplitude and 5Hz frequency. Fig. 21 shows the experimental

TABLE 2. The control performance indexes under different strokes.

Method	s_t =10mm			s_t =20mm			s_t =30mm		
	ST (s)	OS (mm)	IAE (10^{-2})	ST (s)	OS (mm)	IAE (10^{-2})	ST (s)	OS (mm)	IAE (10^{-2})
IMC-PID	0.302	0.094	1.47	0.343	0.116	1.99	0.353	0.126	2.50
LADRC	0.628	0.121	2.56	0.607	0.148	2.80	0.959	0.131	3.76
IMC-PID-MLESO	0.243	0.035	1.22	0.253	0.055	1.65	0.303	0.068	2.00

TABLE 3. The control performance indexes under different cases.

Method	Case 1		Case 2		Case 3		Case 4	
	SD	IAE	SD	IAE	SD	IAE	SD	IAE
IMC-PID	0.031	0.053	0.069	0.123	0.053	0.094	0.133	0.240
LADRC	0.064	0.091	0.093	0.141	0.077	0.127	0.111	0.178
IMC-PID-MLESO	0.023	0.033	0.045	0.076	0.027	0.048	0.037	0.062

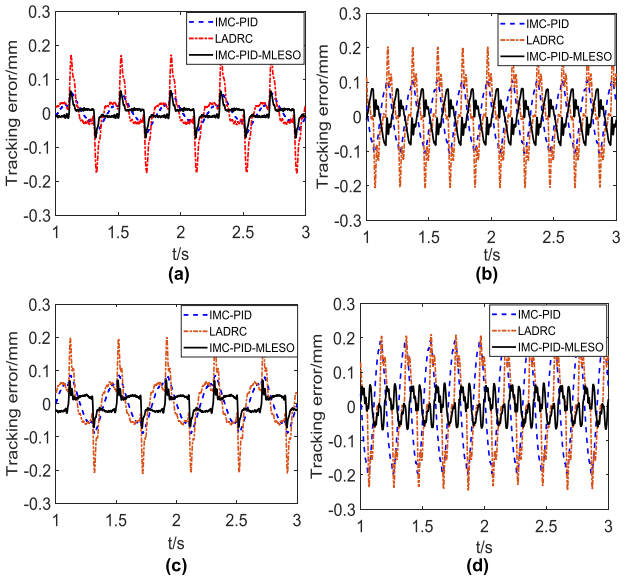

FIGURE 21. Sinusoidal tracking experiment under different cases: (a) Case 1, (b) Case 2, (c) Case 3, (d) Case 4.

curves of tracking error in the tracking stability stage of 1–3s with the control parameters unchanged. Table 3 shows the standard deviation (SD) and IAE of the three control methods in the different cases.

Fig. 21 and Table 3 show that the tracking performance of LADRC is worse than that of IMC-PID and IMC-PID-MLESO. The tracking performance of IMC-PID deteriorates significantly with increasing amplitude or frequency. However, IMC-PID-MLESO remains unaffected by changes in the friction force during sinusoidal tracking and adapts to the amplitude and frequency changes of the input signal. Thus, it achieves satisfactory tracking performance and control robustness.

VI. CONCLUSION

A new method termed IMC-PID-MLESO for PMLSM servo systems was proposed herein to improve the position tracking performance and disturbance rejection ability simultaneously. The control structure of the method incorporates the identified model parameter information into the MLESO design to reduce the estimation burden associated with the total unknown uncertainties and improve the estimation accuracy. Based on the dynamic compensation of the total unknown uncertainties, the PMLSM plant model was transformed into the nominal model of the system. The IMC-PID feedback controller could then perform the closed-loop position control, thereby improving the system stability. Simulation results showed that the proposed method can achieve satisfactory disturbance rejection and position tracking performance simultaneously. For verification, experiments were conducted on a designed experimental platform. The experimental results verify that the IMC-PID-MLESO method has a stronger disturbance rejection ability and higher tracking accuracy than that of the IMC-PID and LADRC.

REFERENCES

[1] S. Zhen, P. Chen, X. Chen, F. Qin, and H. Zhou, "Force ripple modeling and minimizing of an ironless permanent-magnet linear synchronous motor," *Int. J. Precis. Eng. Manuf.*, vol. 20, no. 6, pp. 927–935, Jun. 2019, doi: 10.1007/s12541-019-00065-5.

[2] F. Zhi, M. Zhang, Y. Zhu, and X. Li, "Analysis and elimination of harmonics in force of ironless permanent magnet linear synchronous motor," (in Chinese), *Proc. CSEE*, vol. 37, no. 7, pp. 2101–2109, Apr. 2017, doi: 10.13334/j.0258-8013.pcsee.160737.

[3] M. Wang, L. Li, and D. Pan, "Detent force compensation for PMLSM systems based on structural design and control method combination," *IEEE Trans. Ind. Electron.*, vol. 62, no. 11, pp. 6845–6854, Nov. 2015, doi: 10.1109/TIE.2015.2443096.

[4] E.-J. Park, S.-Y. Jung, and Y.-J. Kim, "A design of optimal interval between armatures in long distance transportation PMLSM for end cogging force reduction," *J. Electr. Eng. Technol.*, vol. 11, no. 2, pp. 361–366, Mar. 2016, doi: 10.5370/JEET.2016.11.2.361.

[5] H.-Y. Jin and X.-M. Zhao, "Extended Kalman filter-based disturbance feed-forward compensation considering varying mass in high-speed permanent magnet linear synchronous motor," *Electr. Eng.*, vol. 101, no. 2, pp. 537–544, Jun. 2019, doi: 10.1007/s00202-019-00802-z.

[6] J. Hu and B. Ding, "Output feedback robust MPC for linear systems with norm-bounded model uncertainty and disturbance," *Automatica*, vol. 108, Oct. 2019, Art. no. 108489, doi: 10.1016/j.automatica.2019.07.002.

[7] J. Hu and B. Ding, "An efficient offline implementation for output feedback min-max MPC," *Int. J. Robust Nonlinear Control*, vol. 29, no. 2, pp. 492–506, Nov. 2018, doi: 10.1002/rnc.4401.

[8] J. G. Kim, C. H. Han, and S. K. Jeong, "Disturbance observer-based robust control against model uncertainty and disturbance for a variable speed refrigeration system," *Int. J. Refrig.*, vol. 116, pp. 49–58, Aug. 2020, doi: 10.1016/j.ijrefrig.2020.03.019.
[9] S. Zaare and M. R. Soltanpour, "The position control of the ball and beam system using state-disturbance observe-based adaptive fuzzy sliding mode control in presence of matched and mismatched uncertainties," *Mech. Syst. Signal Process.*, vol. 150, Mar. 2021, Art. no. 107243, doi: 10.1016/j.ymssp.2020.107243.
[10] J. Yang, S. Li, J. Su, and X. Yu, "Continuous nonsingular terminal sliding mode control for systems with mismatched disturbances," *Automatica*, vol. 49, no. 7, pp. 2287–2291, Jul. 2013, doi: 10.1016/j.automatica.2013.03.026.
[11] M.-H. Tsai and P.-C. Tung, "A disturbance reduction scheme for linear small delay systems with modeling uncertainties," *J. Process Control*, vol. 20, no. 6, pp. 777–786, Jul. 2010, doi: 10.1016/j.jprocont.2010.04.010.
[12] X. Hu, J. Du, G. Zhu, and Y. Sun, "Robust adaptive NN control of dynamically positioned vessels under input constraints," *Neurocomputing*, vol. 318, pp. 201–212, Nov. 2018, doi: 10.1016/j.neucom.2018.08.056.
[13] X. Hu, X. Wei, H. Zhang, W. Xie, and Q. Zhang, "Composite anti-disturbance dynamic positioning of vessels with modelling uncertainties and disturbances," *Appl. Ocean Res.*, vol. 105, Dec. 2020, Art. no. 102404, doi: 10.1016/j.apor.2020.102404.
[14] M. Wang, R. Yang, C. Zhang, J. Cao, and L. Li, "Inner loop design for PMLSM drives with thrust ripple compensation and high-performance current control," *IEEE Trans. Ind. Electron.*, vol. 65, no. 12, pp. 9905–9915, Dec. 2018, doi: 10.1109/TIE.2018.2814014.
[15] R. Wang, F. Man, D. Yan, B. Hu, S. Sun, Q. Chen, and J. Wang, "Research on multi-loop nonlinear control structure and optimization method of PMLSM," *IEEE Access*, vol. 7, pp. 165048–165059, Nov. 2019, doi: 10.1109/ACCESS.2019.2952879.
[16] M. Pirasteh-Moghadam, M. G. Saryazdi, E. Loghman, A. Kamali, and F. Bakhtiari-Nejad, "Development of neural fractional order PID controller with emulator," *ISA Trans.*, vol. 106, pp. 293–302, Nov. 2020, doi: 10.1016/j.isatra.2020.06.014.
[17] S. K. Lakshmanaprabu, M. Elhoseny, and K. Shankar, "Optimal tuning of decentralized fractional order PID controllers for TITO process using equivalent transfer function," *Cognit. Syst. Res.*, vol. 58, pp. 292–303, Dec. 2019, doi: 10.1016/j.cogsys.2019.07.005.
[18] M. B. Milovanović, D. S. Antić, M. T. Milojković, S. S. Nikolić, S. L. Perić, and M. D. Spasić, "Adaptive PID control based on orthogonal endocrine neural networks," *Neural Netw.*, vol. 84, pp. 80–90, Dec. 2016, doi: 10.1016/j.neunet.2016.08.012.
[19] J. Ye, "Adaptive control of nonlinear PID-based analog neural networks for a nonholonomic mobile robot," *Neurocomputing*, vol. 71, nos. 7–9, pp. 1561–1565, Mar. 2008, doi: 10.1016/j.neucom.2007.04.014.
[20] S.-M. Kim and W.-Y. Han, "Induction motor servo drive using robust PID-like neuro-fuzzy controller," *Control Eng. Pract.*, vol. 14, no. 5, pp. 481–487, May 2006, doi: 10.1016/j.conengprac.2005.03.002.
[21] A. Amirkhani, M. Shirzadeh, M. H. Shojaeefard, and A. Abraham, "Controlling wheeled mobile robot considering the effects of uncertainty with neuro-fuzzy cognitive map," *ISA Trans.*, vol. 100, pp. 454–468, May 2020, doi: 10.1016/j.isatra.2019.12.011.
[22] W. Zeng, W. Zhu, T. Hui, L. Chen, J. Xie, and T. Yu, "An IMC-PID controller with particle swarm optimization algorithm for MSBR core power control," *Nucl. Eng. Des.*, vol. 360, Apr. 2020, Art. no. 110513, doi: 10.1016/j.nucengdes.2020.110513.
[23] Z. Xiang, D. Ji, H. Zhang, H. Wu, and Y. Li, "A simple PID-based strategy for particle swarm optimization algorithm," *Inf. Sci.*, vol. 502, pp. 558–574, Oct. 2019, doi: 10.1016/j.ins.2019.06.042.
[24] J. Fiser and P. Zítek, "PID controller tuning via dominant pole placement in comparison with ziegler-nichols tuning," *IFAC-PapersOnLine*, vol. 52, no. 18, pp. 43–48, 2019, doi: 10.1016/j.ifacol.2019.12.204.
[25] E. N. Goncalves, R. M. Palhares, and R. H. C. Takahashi, "A novel approach for H_2/H_∞ robust PID synthesis for uncertain systems," *J. Process Control*, vol. 18, no. 1, pp. 19–26, Jan. 2008, doi: 10.1016/j.jprocont.2007.06.003.
[26] D. Rivera, M. Morari, and S. Skogestad, "Internal model control: PID controller design," *Ind. Eng. Chem. Process Des. Dev.*, vol. 25, no. 1, p. 2163, 1986, doi: 10.1021/i200032a041.
[27] A. Ghosh, T. R. Krishnan, P. Tejaswy, A. Mandal, J. K. Pradhan, and S. Ranasingh, "Design and implementation of a 2-DOF PID compensation for magnetic levitation systems," *ISA Trans.*, vol. 53, no. 4, pp. 1216–1222, Jul. 2014, doi: 10.1016/j.isatra.2014.05.015.
[28] E. Alcala, V. Puig, J. Quevedo, T. Escobet, and R. Comasolivas, "Autonomous vehicle control using a kinematic Lyapunov-based technique with LQR-LMI tuning," *Control Eng. Pract.*, vol. 73, pp. 1–12, Apr. 2018, doi: 10.1016/j.conengprac.2017.12.004.
[29] S. Skogestad, "Simple analytic rules for model reduction and PID controller tuning," *J. Process Control*, vol. 13, no. 4, pp. 291–309, Jun. 2003doi: 10.1016/S0959-1524(02)00062-8.
[30] N. Hamideh, M.-B. Farshad, and J. Abolfazl, "IMC-PID controller design based on loop shaping via LMI approach," *Chem. Eng. Res. Des.*, vol. 24, pp. 170–180, Jun. 2017, doi: 10.1016/j.cherd.2017.06.007.
[31] X. Zhao and Y. Wu, "Backstepping control based on adaptive modified Laguerre ecurrent neural network for permanent magnet linear synchronous motor," *Trans. Chin. Electrotech. Soc.*, vol. 33, no. 10, pp. 2392–2399, May 2018, doi: 10.19595/j.cnki.1000-6753.tces.171239.
[32] Y. Wu and X. Zhao, "Adaptive backstepping control based on functional link radial basis function neural network for PMLSM," *Trans. Chin. Electrotech. Soc.*, vol. 33, no. 17, pp. 4044–4051, Sep. 2018, doi: 10.19595/j.cnki.1000-6753.tces.180019.
[33] J. Han, "Active disturbance rejection controller and its applications," (in Chinese), *Control Decis.*, vol. 13, no. 1, pp. 19–23, 1998.
[34] J. Han, "From PID to active disturbance rejection control," *IEEE Trans. Ind. Electron.*, vol. 56, no. 3, pp. 900–906, Mar. 2009, doi: 10.1109/TIE.2008.2011621.
[35] H. Feng and B.-Z. Guo, "A new active disturbance rejection control to output feedback stabilization for a one-dimensional anti-stable wave equation with disturbance," *IEEE Trans. Autom. Control*, vol. 62, no. 8, pp. 3774–3787, Aug. 2017, doi: 10.1109/TAC.2016.2636571.
[36] Z. Gao, "Scaling and bandwidth-parameterization based controller tuning," in *Proc. Amer. Control Conf.*, Denver, CO, USA, 2003, pp. 4989–4996, doi: 10.1109/ACC.2003.1242516.
[37] C. Wang, L. Quan, S. Zhang, H. Meng, and Y. Lan, "Reduced-order model based active disturbance rejection control of hydraulic servo system with singular value perturbation theory," *ISA Trans.*, vol. 67, pp. 455–465, Mar. 2017, doi: 10.1016/j.isatra.2017.01.009.
[38] B. Gao, J. Shao, and X. Yang, "A compound control strategy combining velocity compensation with ADRC of electro-hydraulic position servo control system," *ISA Trans.*, vol. 53, no. 6, pp. 1910–1918, Nov. 2014, doi: 10.1016/j.isatra.2014.06.011.
[39] S. Li, K. Zhang, J. Li, and C. Liu, "On the rejection of internal and external disturbances in a wind energy conversion system with direct-driven PMSG," *ISA Trans.*, vol. 61, pp. 95–103, Mar. 2016, doi: 10.1016/j.isatra.2015.12.014.
[40] C. Liu, G. Luo, Z. Chen, and W. Tu, "Measurement delay compensated LADRC based current controller design for PMSM drives with a simple parameter tuning method," *ISA Trans.*, vol. 101, pp. 482–492, Jun. 2020, doi: 10.1016/j.isatra.2020.01.027.
[41] J. Huang, P. Ma, G. Bao, F. Gao, and X. Shi, "Research on position servo system based on fractional-order extended state observer," *IEEE Access*, vol. 8, pp. 102748–102756, Jun. 2020, doi: 10.1109/ACCESS.2020.2997407.
[42] C. Fu and W. Tan, "Tuning of linear ADRC with known plant information," *ISA Trans.*, vol. 65, pp. 384–393, Nov. 2016, doi: 10.1016/j.isatra.2016.06.016.
[43] H. Feng and B.-Z. Guo, "Active disturbance rejection control: Old and new results," *Annu. Rev. Control*, vol. 44, pp. 238–248, May 2017, doi: 10.1016/j.arcontrol.2017.05.003.
[44] J. Gai, Q. Huang, S. Huang, W. Liu, T. Zhou, and X. Pan, "Active-disturbance rejection controller for permanent magnet synchronous motor based on model compensation," (in Chinese), *J. Zhejiang Univ. (Eng. Sci.)*, vol. 48, no. 4, pp. 581–588, Apr. 2014, doi: 10.3785/j.issn.1008-973X.2014.04.004.
[45] Z.-G. Liu and S.-H. Li, "Active disturbance rejection controller based on permanent magnetic synchronous motor model identification and compensation," (in Chinese), *Proc. Chin. Soc. Elect. Eng.*, vol. 28, no. 24, pp. 118–123, Aug. 2008, doi: 10.13334/j.0258-8013.pcsee.2008.24.015.
[46] P. Li and G. Zhu, "IMC-based PID control of servo motors with extended state observer," *Mechatronics*, vol. 62, Oct. 2019, Art. no. 102252, doi: 10.1016/j.mechatronics.2019.102252.